 doi:10.20944/preprints202105.0584.v1

Article

Hypergolic synthesis of inorganic materials by the reaction of metallocene dichlorides with fuming nitric acid at ambient conditions: the case of photocatalytic titania

Nikolaos Chalmpes [1], Georgios Asimakopoulos [1], Maria Baikousi [1], Athanasios B. Bourlinos [2,*], Michael A. Karakassides [1], and Dimitrios Gournis [1,*]

[1] Department of Materials Science & Engineering, University of Ioannina, 45110 Ioannina, Greece; chalmpesnikos@gmail.com (N.C.); asimakopoulos.geo@gmail.com (G.A.); mariabaikousi@gmail.com (M.B.); mkarakas@uoi.gr (M.A.K.)

[2] Physics Department, University of Ioannina, 45110 Ioannina, Greece

* Correspondence: bourlino@uoi.gr (A.B.B.); dgourni@uoi.gr (D.G.); Tel.: +30-26510-07141 (D.G.)

Abstract: Hypergolic materials synthesis is a new preparative technique in materials science that allows a wide range of carbon or inorganic solids with useful properties to be obtained. Previously we have demonstrated that metallocenes are versatile reagents in the hypergolic synthesis of inorganic materials, such as γ-Fe_2O_3, Cr_2O_3, Co, Ni and alloy CoNi. Here, we take one step further by using metallocene dichlorides as precursors for the hypergolic synthesis of additional inorganic phases, such as photocatalytic titania. Metallocene dichlorides are closely related to metallocenes, thus expanding the arsenal of organometallic compounds that can be used in hypergolic materials synthesis. In the present case, we show that hypergolic ignition of the titanocene dichloride-fuming nitric acid pair results in the fast and spontaneous formation of titania nanoparticles at ambient conditions in the form of anatase-rutile mixed phases. The obtained titania shows good photocatalytic activity towards Cr(VI) removal (100 % within 9 h), the latter being dramatically enhanced after calcination of the powder at 500 °C (100 % within 3 h). Worth noting, this performance was found to be comparable to that of commercially available P25 TiO_2 under identical conditions. The cases of zirconocene, hafnocene and molybdocene dichlorides are complementary discussed in this work, aiming to show the wider applicability of metallocene dichlorides in the hypergolic synthesis of inorganic materials (ZrO_2, HfO_2, MoO_2).

Keywords: hypergolic materials synthesis; metallocene dichlorides; fuming nitric acid; photocatalytic titania; Cr(VI) removal

1. Introduction

Progress in materials science largely depends on new synthesis methods and techniques. These typically include solid–state, ball–milling, arc–discharge, plasma, pyrolytic, template synthesis, nanolithography, high pressure–high temperature (HPHT), sol–gel, freeze–drying, microemulsion, precipitation, borohydride reduction, thermolysis, hot-injection, sonochemical, hydrothermal, chemical vapor deposition, sputtering, flame spray pyrolysis, electrochemical and microwave synthesis [1-3]. In spite of the large variety of existing techniques today, there is an ever increasing demand for new synthesis methods in materials science that will deal with needs not met by the previous ones.

Recently our group has introduced hypergolic materials synthesis as a radically new preparative method in materials science [4-12]. At the heart of this new technique are hypergolic reactions. In hypergolic reactions, a fuel (organic, inorganic or organometallic) and a strong oxidizer (fuming nitric acid, sodium peroxide, chlorine or bromine) ignite rapidly and spontaneously upon contact at room temperature and atmospheric

Preprints (www.preprints.org) | NOT PEER-REVIEWED | Posted: 24 May 2021 doi:10.20944/preprints202105.0584.v1

pressure without external stimuli (spark, lighter or match). Spontaneity results from the exothermic character of hypergolic reactions ($\Delta H < 0$) as well as the release of a large amount of gaseous products ($\Delta S > 0$), that eventually lead to negative free energy changes ($\Delta G = \Delta H - T\,\Delta S < 0$). On the other hand, the fast kinetics likely results from the fact that hypergolic reactions are usually spin-allowed, i.e., no spin change takes place as moving from the reactants to the products, thus ensuring a small activation energy (E_a).

Certain advantages of hypergolic materials synthesis are: i) simplicity and easy operation (e.g., one has to merely bring into contact two reagents at ambient conditions), ii) generality towards both carbon and inorganic materials synthesis, iii) the targeted material (carbon or inorganic) is formed rapidly (within seconds) and spontaneously at ambient conditions upon contact of the reagents, iv) the released hypergolic energy can be further converted into useful work (chemical, mechanical, photovoltaic, thermoelectric or heating fluids), and, v) since hypergolic reactions and rocket fuel propellants are closely related [10], hypergolic materials synthesis provides a practical way of converting disposed rocket fuel (also known as "mélange") into useful material (in other words, it provides an alternative rocket fuel waste management other than feedstock in chemical industry or fertilizers; see links: https://www.osce.org/secretariat/57488 and https://www.osce.org/files/f/documents/8/f/35905.pdf, last accessed on 8/4/2021). As a keynote remark, hypergolic materials synthesis not only allows a fast and spontaneous formation of a wide range of nanomaterials at ambient conditions but also produces useful energy in the process. This clearly differentiates from other preparative techniques where the formation of a material might require prolonged heating at high temperature (i.e., a time- and energy-consuming process).

At this point it should be emphasized that the method is safe to run at small scale in the lab; however, for large scale synthesis it would be necessary to build a pilot reactor that would borrow basic ideas from rocket fuel engineering. Hence, such a reactor could be simply made up of an ignition chamber simultaneously connected to a fuel tank and an oxidizer tank, just like in rockets [13]. Although the method is still going through its first steps, we believe that it has a great potential to develop similarly to the flame spray pyrolysis technique in the near future. For instance, flame spray pyrolysis, which had started timidly decades ago due to serious hazards involved in the process (flammable methane, hot flames etc.), is now widely used in labs and industry thanks to technical upgrades overtime. Currently, several important materials (carbon black, fumed silica, P25 titania) are routinely produced *via* flame spray pyrolysis [14].

Although the majority of examples provided from our group pertain to carbon, hypergolic materials synthesis can be extended beyond carbon for the synthesis of inorganic materials as well. For instance, in a previous work we have presented the rapid synthesis of inorganic materials (γ-Fe_2O_3, Cr_2O_3, Co, Ni, alloy CoNi) by the hypergolic ignition of suitable metallocenes with fuming nitric acid [9]. Herein we further expand the gallery of available nanostructures by using closely related metallocene dichlorides and fuming HNO_3 as the starting reagents, with particular emphasis on photocatalytic titania [15,16]. The latter is obtained by the hypergolic ignition of the titanocene dichloride-fuming HNO_3 pair, thus resulting in nanocrystalline titania composed of anatase-rutile polymorphs. The effectiveness of the titania nanoparticles in the photocatalytic removal of hexavalent chromium from water is assessed for both as-made and calcined powders, showing a highly efficient removal in the latter case (100 % within 3 h). This effect is comparable to that of benchmark P25 TiO_2 under identical conditions. Besides titanocene dichloride, the related zirconocene, hafnocene and molybdocene dichlorides also react hypergolically with fuming nitric acid to afford the corresponding ZrO_2, HfO_2 and MoO_2 phases, hence demonstrating the general character of the method. Overall, metallocene dichlorides together with metallocenes, thanks to a diverse structure and composition, appear to be versatile reagents for the hypergolic synthesis of a wide range of inorganic materials with useful properties (magnetic, photocatalytic etc.).

2. Materials and Methods

Preprints (www.preprints.org) | NOT PEER-REVIEWED | Posted: 24 May 2021 doi:10.20944/preprints202105.0584.v1

Synthesis was conducted in a fume hood with ceramic tile bench using small amount of reagents. In a typical procedure, a glass test tube (diameter: 1.6 cm; length: 16 cm) was charged with 0.5 g $TiCp_2Cl_2$ (titanocene dichloride, 97 % Sigma–Aldrich, St. Louis, MO, USA) followed by the dropwise addition of 0.75 mL fuming nitric acid (100 % Sigma–Aldrich, St. Louis, MO, USA). Both reagents reacted hypergolicly upon contact to afford a solid residue within the tube. The residue was collected and washed successively with water, acetone and tetrahydrofuran prior to drying at 80 °C (thereafter denoted as as-made sample or as–made titania). Water helps to remove residual acid after reaction, whereas acetone and tetrahydrofuran help to wash off any unreacted titanocene dichloride which is soluble in both solvents. The hypergolic ignition of the organometallic compound by fuming HNO_3 is shown in Figure 1. Calcined titania (or calcined sample) was obtained by heat treatment of the as-made titania at 500 °C for 1 h under air in a box oven. Due to the general character of the method, even more inorganic materials could be foreseen using suitable metallocene dichlorides and fuming nitric acid as described above.

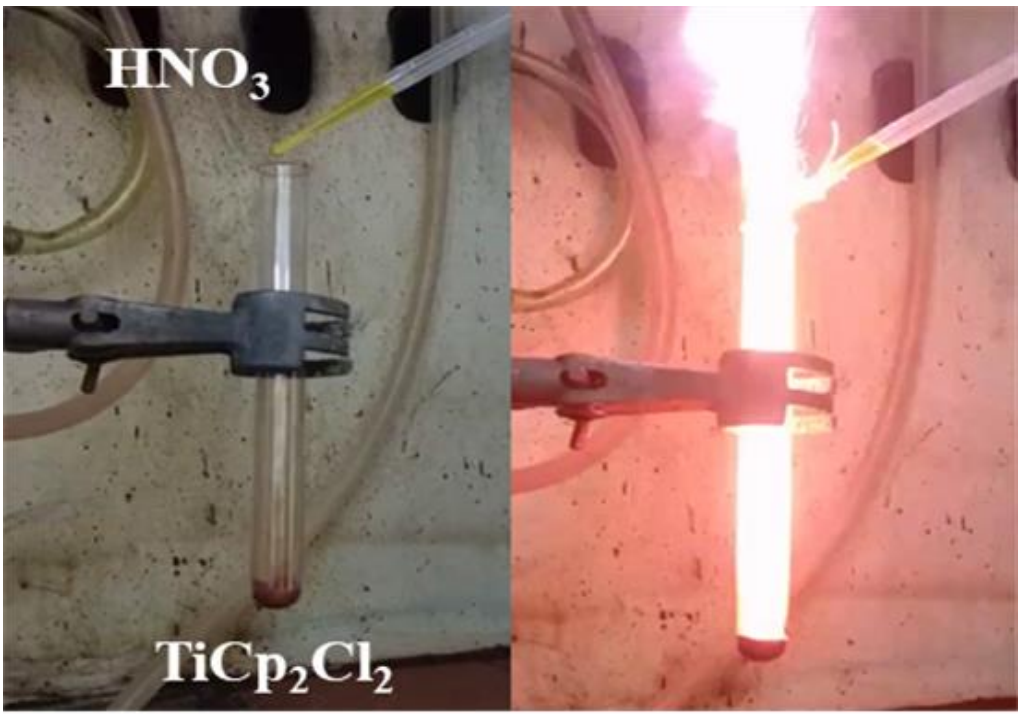

Figure 1. Dropwise addition of fuming nitric acid into titanocene dichloride in a test tube triggers a spontaneous ignition towards titania formation.

Powder X-ray diffraction (XRD) was performed using background-free Si wafers and Cu Kα radiation from a Bruker Advance D8 diffractometer (Bruker, Billerica, MA, USA). Raman spectra were recorded with a micro–Raman system RM 1000 Renishaw using a laser excitation line at 532 nm. Atomic force microscopy (AFM) images were collected on silicon wafers in tapping mode with a Bruker Multimode 3D Nanoscope (Ted Pella Inc., Redding, CA, USA).

UV–Visible spectra of chromium solutions were recorded in quartz vesicle with a UV–2401(PC) –Shimadzu spectrophotometer. The photocatalytic experiments were carried out in a photoreactor containing a quartz cylindrical tube (diameter: 3.5 cm, height: 18 cm) placed inside a stainless–steel cooling bath. A magnetic stirrer was used for mixing the solutions and it was located under the photoreactor. Two UV–C lamps, each with roughly 18 W maximum output power and the peak wavelength at 253.7 nm, were used as light sources and fitted to the side of the quartz tube. The interior of the bath was tucked with aluminum foil to increase the illumination of the samples while the reactor

 doi:10.20944/preprints202105.0584.v1

temperature was kept constant at 25 °C. Benchmark P25 TiO_2, which is a reference material in photocatalysis, was tested as well in our experiments under identical conditions for comparison reasons.

3. Results and Discussion

3.1. Synthesis and characterization

The hypergolic reaction between titanocene dichloride and fuming nitric acid results in the simultaneous formation of carbon and titania phases in the as–made sample (N_2 BET surface area: 52 m^2/g). The titanium-containing organometallic compound serves as the source of titania, whereas the attached cyclopentadienyl groups serve as the source of residual carbon [9]. Based on thermal gravimetric analysis in air, the carbon content of the as-made sample reaches the value of 40 % with the rest 60 % being TiO_2. Accordingly, an additional heat treatment step at 500 °C for 1 h under air is necessary in order to free the inorganic phase from residual carbon (N_2 BET surface area: 62 m^2/g).

AFM study of the as-made titania shows the presence of spherical nanoparticles with an average size of 12 nm (Figure 2a). In addition to the nanoparticles we also observe impaired, irregular–shaped carbon nanosheets with thickness of about 2 nm (Figure 2b). Therefore the as–made sample should be better described as an admixture of titania and carbon phases. The two phases co–exist separately in large part of the sample in the form of a heterogeneous mixture, however, some nanosheets spotted with titania nanoparticles were also observed (not shown).

Preprints (www.preprints.org) | NOT PEER-REVIEWED | Posted: 24 May 2021 doi:10.20944/preprints202105.0584.v1

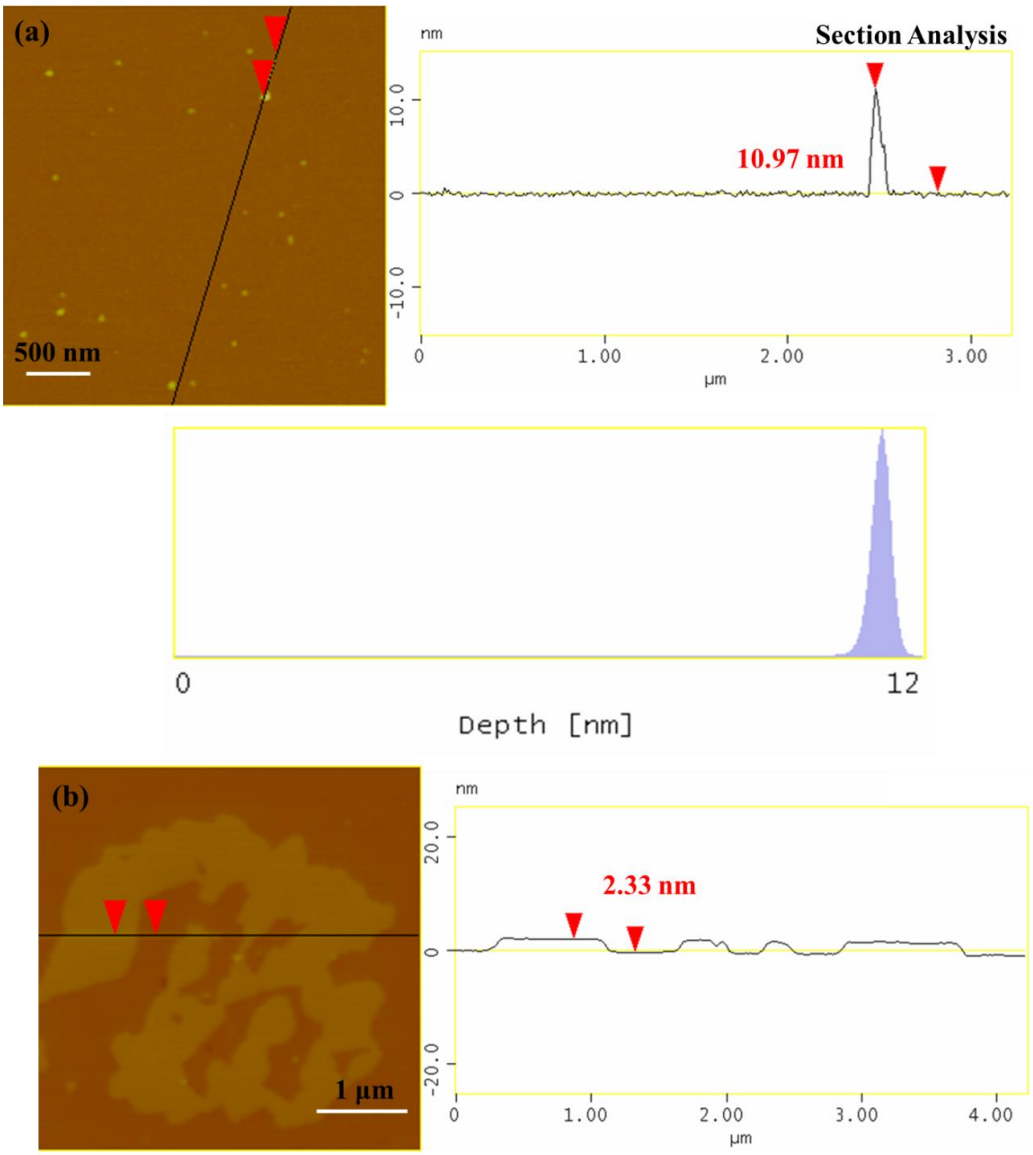

Figure 2. (a) AFM cross section analysis profile and depth analysis–histogram of the titania nanoparticles in the as–made sample. (b) The sample additionally contains impaired, irregular-shaped carbon nanosheets of thickness ca. 2 nm.

In order to completely remove carbon, the sample was calcined at 500 °C in air to afford pure titania. AFM analysis in this case revealed the exclusive presence of spherical titania nanoparticles of about the same size as for the parent sample within statistical error (Figure 3). Thus, heat treatment leaves nearly unaffected the size and morphology of the TiO_2 nanoparticles, but nevertheless brings forth changes in the phase composition of titania, as discussed in the next paragraph.

Preprints (www.preprints.org) | NOT PEER-REVIEWED | Posted: 24 May 2021 doi:10.20944/preprints202105.0584.v1

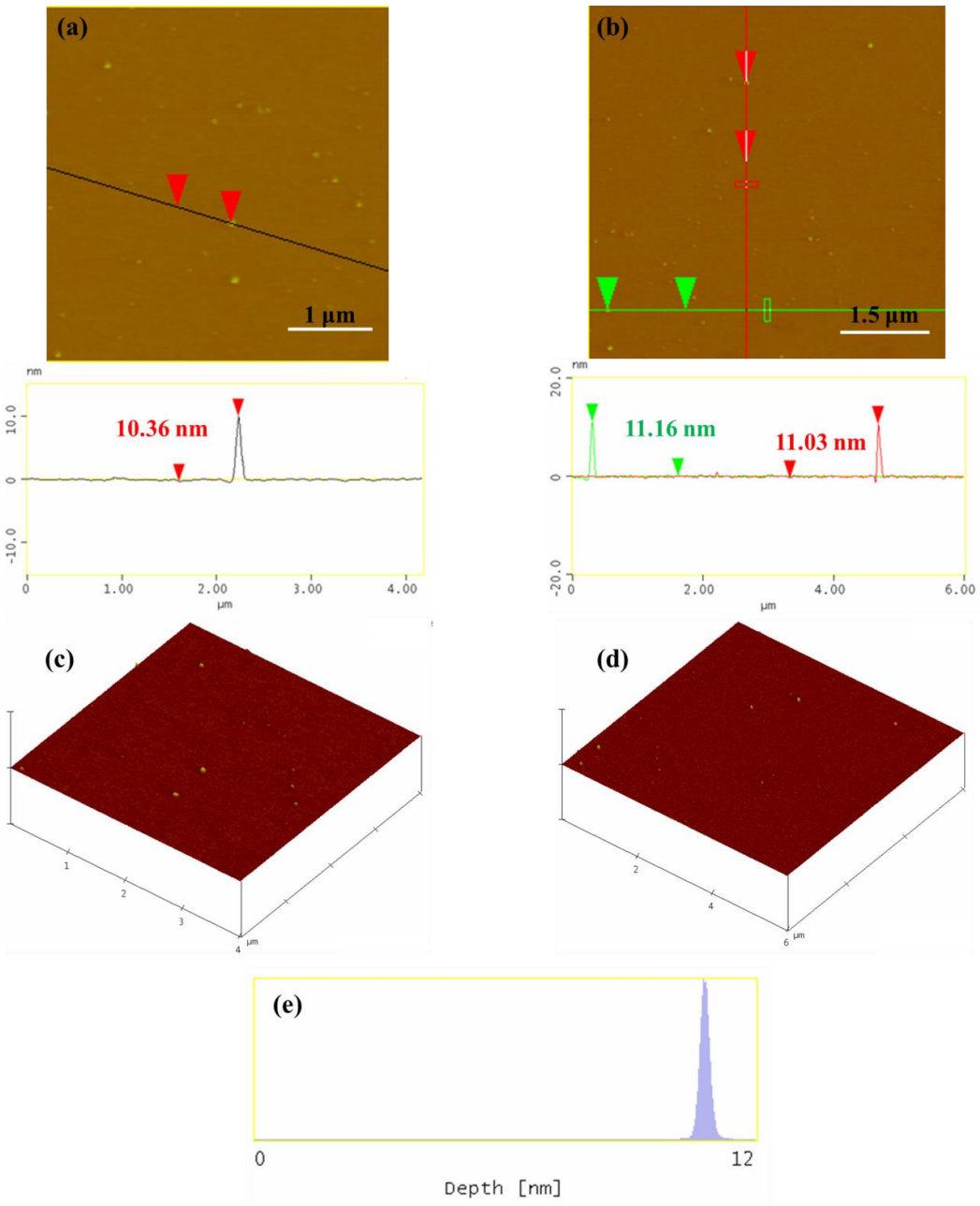

Figure 3. Representative AFM cross section analysis profile (a, b), 3D morphology (c, d) and particle size distribution histogram (e) of calcined titania.

The crystalline structure and phase composition of the as–made and calcined titanias were studied by X–ray diffraction (Figure 4). In both cases, the titania consists of the anatase and rutile mixed phases, but at different ratios. Based on Rietveld analysis, the as-made titania contains 85 % anatase and 15 % rutile, whereas the calcined one 70 % anatase and 30 % rutile, as a result of partial anatase-to-rutile thermal transformation at 500 °C [17]. Interestingly, the anatase/rutile ratio for the as-made sample is close to that of photocatalytic Degussa P25–TiO_2 (80/20) [18], whereas that of calcined sample close to the literature reported values for optimal TiO_2 photoreactivity (60/40) [19,20]. Note that it was difficult to detect carbon in the XRD pattern of the as-made titania. This stems from three reasons: i) poorly crystalline carbon (e.g., amorphous carbon) usually gives broad and small intensity (002) reflections in X–rays, ii) superimposition of the (002) carbon and (101) anatase peaks near 25°, and, iii) phase-contrast between the lighter carbon and heavier titania. Nevertheless, the presence of carbon in the as-made sample is clearly confirmed by Raman spectroscopy below.

Preprints (www.preprints.org) | NOT PEER-REVIEWED | Posted: 24 May 2021 doi:10.20944/preprints202105.0584.v1

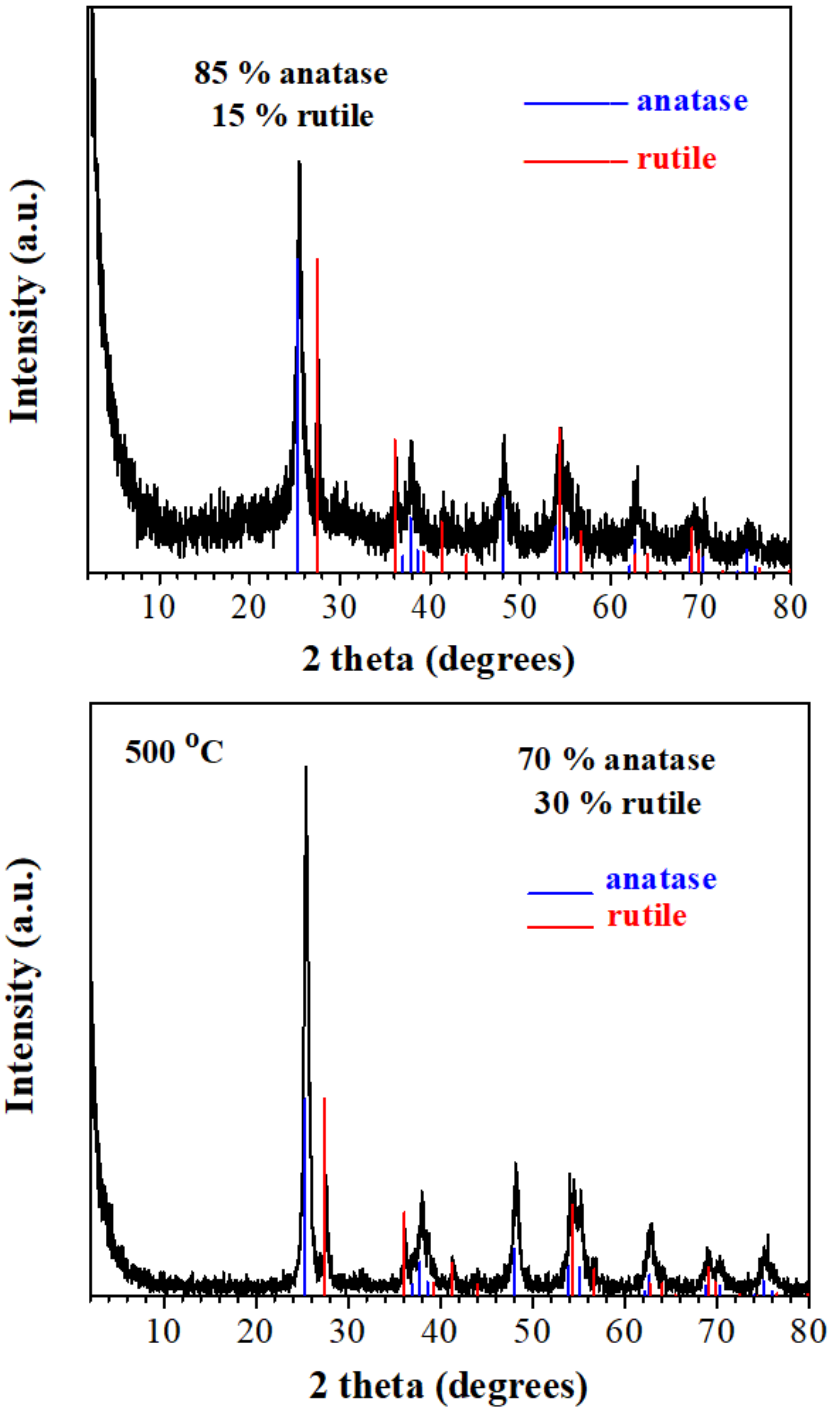

Figure 4. XRD patterns of the as-made (top) and calcined (bottom) titania samples showing the anatase and rutile phases.

The Raman spectrum of the as-made sample shows the simultaneous presence of TiO_2 and carbon (Figure 5 & inset). Titania is evidenced by an intense band at 145 cm^{-1} followed by three smaller intensity bands at 640, 515 and 395 cm^{-1} and a very weak shoulder just less below 200 cm^{-1} [21,22]. These peaks correspond to the five Raman active modes of anatase, and overall, the spectrum matches well that of Degussa P25 [22]. On the other hand, carbon shows the characteristic G and D bands at 1588 cm^{-1} and 1362 cm^{-1}, respectively [23]. Based on the broadness and relative intensity ratio (I_D/I_G = 0.75) of the two bands we can safely conclude that carbon is in amorphous state. In sharp contrast, crystalline graphite displays narrower Raman lines with I_D/I_G ratio close to 0.2. In respect to the calcined sample, this still shows the titania Raman peaks, however, the

Preprints (www.preprints.org) | NOT PEER-REVIEWED | Posted: 24 May 2021 doi:10.20944/preprints202105.0584.v1

characteristic G and D carbon bands completely disappear (Figure 5). This fact signals the sole presence of pure titania in the calcined sample.

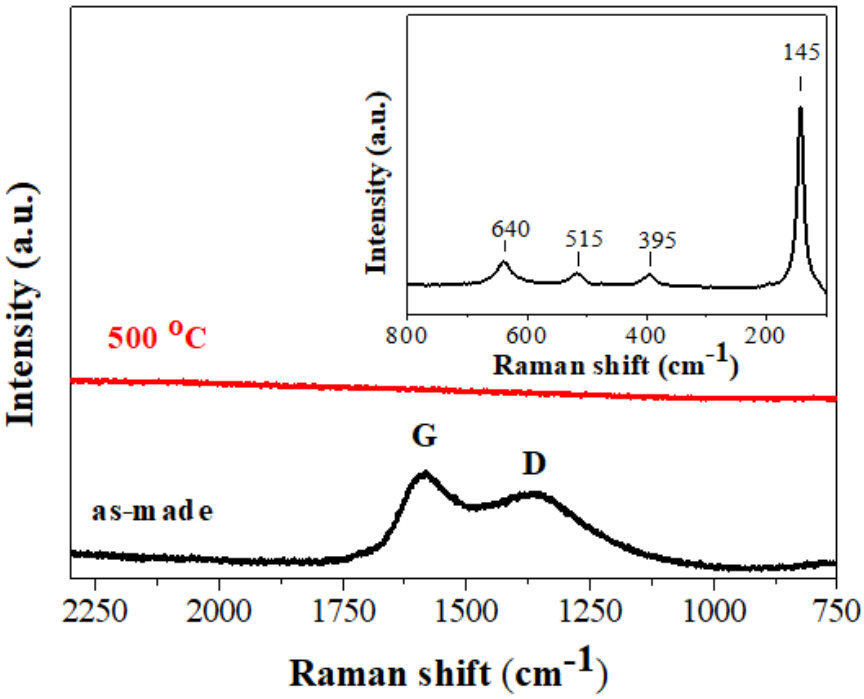

Figure 5. Raman spectra of the as-made and calcined titanias in the carbon region. The characteristic Raman peaks of titania are shown as inset.

Likewise titanocene dichloride, the analogous zirconocene, hafnocene and molybdocene dichlorides ($ZrCp_2Cl_2$ 98 %, $HfCp_2Cl_2$ 98 % and $MoCp_2Cl_2$ 95 % from Sigma–Aldrich, St. Louis, MO, USA) also ignite rapidly and spontaneously with fuming HNO_3 at ambient conditions (Figure 6) to give the corresponding ZrO_2, HfO_2 and MoO_2 phases with characteristic reflections in their XRD patterns (Figure 7). Similarly to the titania case, all the as-made samples additionally contained ca. 40 % carbon that, however, could be easily removed by calcination. Therefore, metallocene dichlorides rather seem to be a general class of organometallic precursors towards the hypergolic synthesis of diverse inorganic materials.

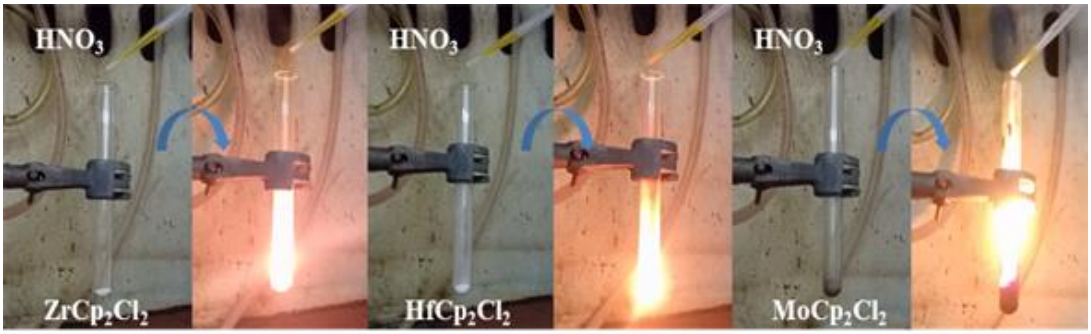

Figure 6. Hypergolic ignition of zirconocene, hafnocene and molybdocene dichlorides by fuming HNO_3.

Preprints (www.preprints.org) | NOT PEER-REVIEWED | Posted: 24 May 2021 doi:10.20944/preprints202105.0584.v1

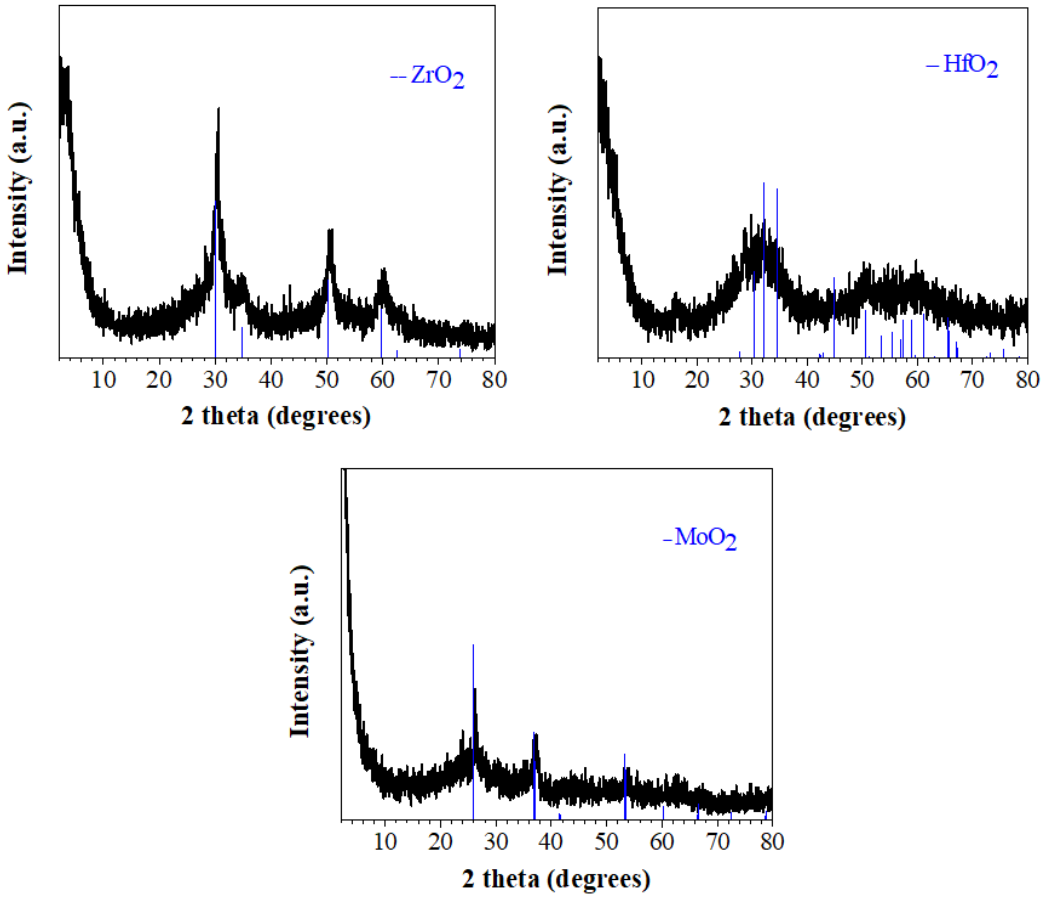

Figure 7. XRD patterns of the ZrO_2, HfO_2 and MoO_2 phases derived through hypergolic ignition of the corresponding $ZrCp_2Cl_2$, $HfCp_2Cl_2$ and $MoCp_2Cl_2$ organometallic compounds by fuming nitric acid.

3.2. Photocatalytic activity of titania towards Cr(VI) removal

Since the anatase-to-rutile ratio in the as-made and calcined samples is close to those of photoreactive TiO_2 [18-20], both titanias were tested successfully in the removal of toxic hexavalent chromium [24] from water under UV irradiation. Ultraviolet light matches the energy band-gap of TiO_2, thus triggering electron transfer from the valence band to the conduction band of the solid [25,26]. The electrons sitting in the conduction band are then available to reduce the highly toxic Cr(VI) species into relatively harmless Cr(III) [25,26]. Thus, ultraviolet light is necessary in order to switch-on the photocatalytic activity of titania. Although sunlight is the main source of UV radiation making up nearly 5 % of the solar spectrum, in our work we have used UV lamps for ensuring controlled experimental conditions throughout the whole process.

The kinetics of Cr(VI) removal with or without UV irradiation at room temperature for both the as-made and calcined samples is depicted in Figure 8, top. Solutions of 50 mL each, containing 9 mg of titania (as made or calcined) and initial Cr(VI) concentration of 5.5 mg/L at pH = 3 (e.g., acidic industrial wastewaters), were used to carry out the experiments [27,28]. Accordingly, total Cr(VI) removal is achieved within 9 hours for the as–made titania and within 3 hours for the calcined titania under UV irradiation (Figure 8, top; closed–red & blue symbols). On the other hand, as expected, the measurements at room temperature for the two materials without UV irradiation show insignificant capability for the removal of hexavalent chromium from the aqueous solution (Figure 8, top; open–red & blue symbols). Also noticeable is the fact that the combination of acid environment and UV irradiation in the absence of titania led to an even less removal of ca. 10 %, thus demonstrating the active role of TiO_2 in the photocatalytic process. For

Preprints (www.preprints.org) | NOT PEER-REVIEWED | Posted: 24 May 2021 doi:10.20944/preprints202105.0584.v1

comparison reasons [29], the efficiency of the commercial TiO_2 nanoparticles, AEROXIDE® TiO_2 P25 (99.5%, EVONIK, Tokyo, Japan) under identical conditions is also presented (Figure 8, bottom). In this case, the total Cr(VI) removal under UV irradiation is achieved within 2 hours, thus being comparable to that of calcined titania.

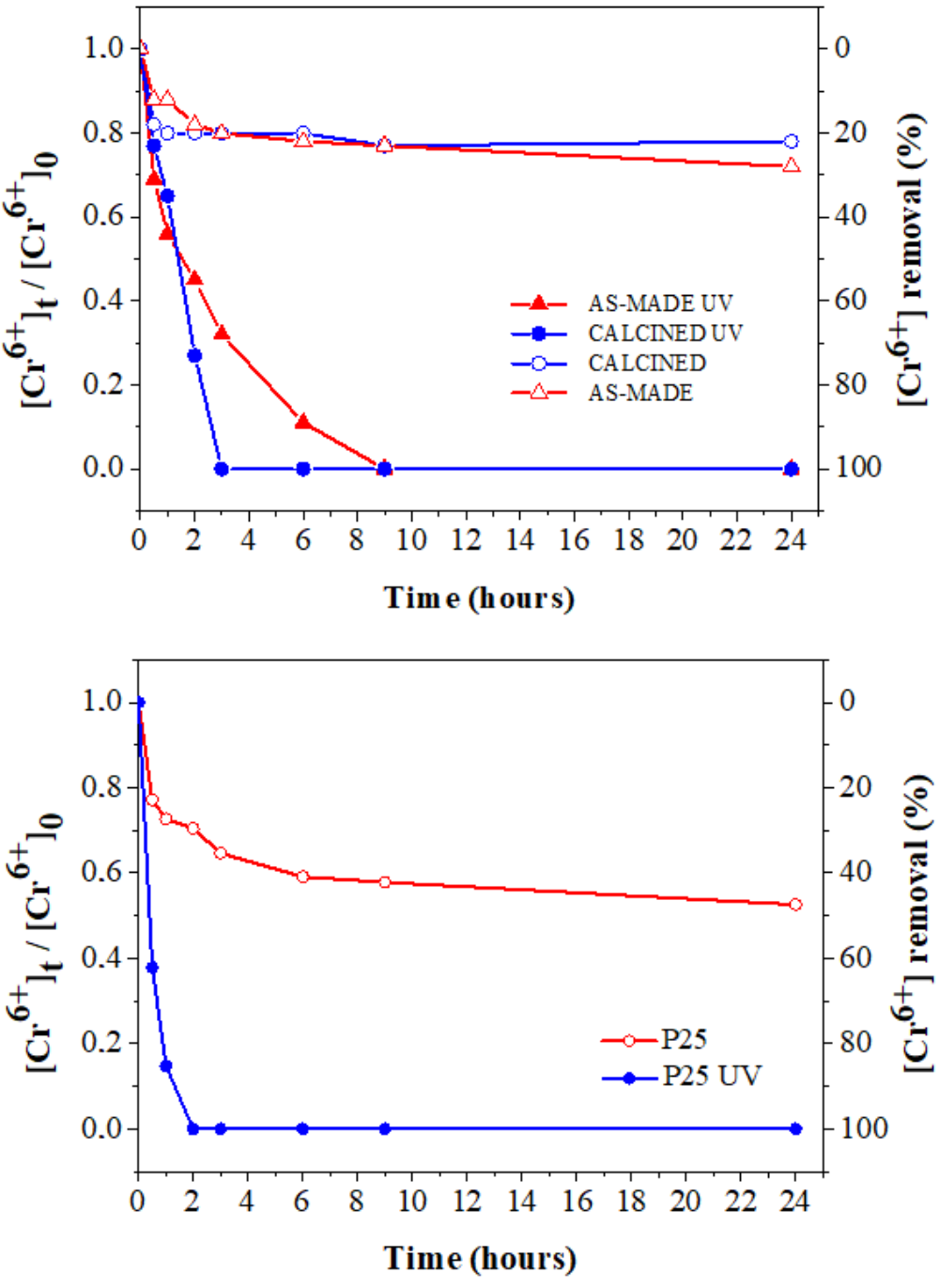

Figure 8. Effect of contact time on the Cr(VI) removal from aqueous solution by the as-made and calcined titanias (top) and P25 TiO_2 (bottom) under UV irradiation (closed–red & blue symbols) and without UV irradiation (open–red & blue symbols).

As it has been shown previously, both as-made and calcined titanias possess comparable nanoparticle sizes and specific surface areas. In addition, the corresponding anatase-to-rutile ratios fall within the expected range of photoreactive titania (typically 60–80 % anatase and 20–40 % rutile). Based on these grounds, the higher photocatalytic

 doi:10.20944/preprints202105.0584.v1

performance of calcined titania should be then ascribed to the high purity of the sample which is void of carbon (e.g., neat titania).

4. Conclusions

Hypergolic materials synthesis is a fresh preparative technique in materials science that, however, needs further basic and technical studies before implementation in a lab- or industrial–scale. In an effort to explore more chemical options in this context, we have presented here the hypergolic ignition of titanocene, zirconocene, hafnocene and molybdocene dichlorides by fuming nitric acid towards the fast and spontaneous formation of the corresponding TiO_2, ZrO_2, HfO_2 and MoO_2 phases at ambient conditions. Particular emphasis was given on the titanocene dichloride–fuming HNO_3 pair, which resulted in the formation of nanocrystalline photocatalytic titania composed of the anatase-rutile mixed phases. The photocatalytic activity of the solid before and after calcination was evaluated in Cr(VI) removal from aqueous solution under UV irradiation. High photocatalytic performance was observed for the calcined sample (100 % removal within 3 h) probably due to the higher purity of the titania phase (e.g., carbon–free). Worth noting, the photocatalytic activity of calcined titania was comparable to that of benchmark P25 TiO_2 under identical conditions. To sum up, metallocene dichlorides, due to a diverse composition, come to expand the chemical possibilities of hypergolic materials synthesis in the manufacture of a larger variety of functional materials with interesting properties.

Author Contributions: Conceptualization, A.B.B.; methodology, N.C., A.B.B.; M.A.K., and D.G.; validation, A.B.B., N.C., G.A., M.B., M.A.K., and D.G.; investigation, A.B.B., N.C., D.M., K.S., M.A.K., and D.G.; data curation, N.C., A.B.B., G.A., M.B., M.A.K., and D.G.; writing-original draft preparation, A.B.B. and N.C. and writing-review and editing, N.C., A.B.B. and D.G.; supervision, A.B.B. and D.G. All authors have read and agreed to the published version of the manuscript.

Funding: This study was funded by the project "National Infrastructure in Nanotechnology, Advanced Materials and Micro-/Nanoelectronics" (MIS-5002772) which was implemented under the action "Reinforcement of the Research and Innovation Infrastructure", funded by the Operational Programme "Competitiveness, Entrepreneurship and Innovation" (NSRF 2014-2020), and co-financed by Greece and the European Union (European Regional Development Fund). N. C. gratefully acknowledges the IKY foundation for the financial support. This research was also co-financed by Greece and the European Union (European Social Fund-ESF) through the Operational Programme "Human Resources Development, Education and Lifelong Learning" in the context of the project "Strengthening Human Resources Research Potential via Doctorate Research" (MIS-5000432), implemented by the State Scholarships Foundation (IKY).

Institutional Review Board Statement: Not applicable.

Informed Consent Statement: Not applicable.

Data Availability Statement: The data presented in this study are available on request from the corresponding author.

Acknowledgments: The authors greatly acknowledge Dr. Ch. Papachristodoulou for the XRD measurements.

Conflicts of Interest: The authors declare no conflict of interest.

References

1. Tavakoli, A.; Sohrabi, M.; Kargari, A. A review of methods for synthesis of nanostructured metals with emphasis on iron compounds. *Chemical Papers* **2007**, *61*, 151-170.
2. Ganachari, S.V.; Banapurmath, N.R.; Salimath, B.; Yaradoddi, J.S.; Shettar, A.S.; Hunashyal, A.M.; Venkataraman, A.; Patil, P.; Shoba, H.; Hiremath, G.B. Synthesis techniques for preparation of nanomaterials. In *Handbook of Ecomaterials*, Martínez, L.M.T., Kharissova, O.V., Kharisov, B.I., Eds.; Springer International Publishing: Cham, 2017; pp. 1-21.
3. Ayuk, E.; Mariagoretti, U.; Samuel, A. A review on synthetic methods of nanostructured materials. *Chemistry Research Journal* **2017**, *2*, 97-123.
4. Baikousi, M.; Chalmpes, N.; Spyrou, K.; Bourlinos, A.B.; Avgeropoulos, A.; Gournis, D.; Karakassides, M.A. Direct production of carbon nanosheets by self-ignition of pyrophoric lithium dialkylamides in air. *Materials Letters* **2019**, *254*, 58-61.
5. Chalmpes, N.; Spyrou, K.; Bourlinos, A.B.; Moschovas, D.; Avgeropoulos, A.; Karakassides, M.A.; Gournis, D. Synthesis of highly crystalline graphite from spontaneous ignition of in situ derived acetylene and chlorine at ambient conditions. *Molecules* **2020**, *25*, 297.
6. Chalmpes, N.; Asimakopoulos, G.; Spyrou, K.; Vasilopoulos, K.C.; Bourlinos, A.B.; Moschovas, D.; Avgeropoulos, A.; Karakassides, M.A.; Gournis, D. Functional carbon materials derived through hypergolic reactions at ambient conditions. *Nanomaterials* **2020**, *10*, 566.
7. Chalmpes, N.; Spyrou, K.; Vasilopoulos, K.C.; Bourlinos, A.B.; Moschovas, D.; Avgeropoulos, A.; Gioti, C.; Karakassides, M.A.; Gournis, D. Hypergolics in carbon nanomaterials synthesis: new paradigms and perspectives. *Molecules* **2020**, *25*, 2207.
8. Chalmpes, N.; Tantis, I.; Bakandritsos, A.; Bourlinos, A.B.; Karakassides, M.A.; Gournis, D. Rapid carbon formation from spontaneous reaction of ferrocene and liquid bromine at ambient conditions. *Nanomaterials* **2020**, *10*, 1564.
9. Chalmpes, N.; Bourlinos, A.B.; Šedajová, V.; Kupka, V.; Moschovas, D.; Avgeropoulos, A.; Karakassides, M.A.; Gournis, D. Hypergolic materials synthesis through reaction of fuming nitric acid with certain cyclopentadienyl compounds. *C* **2020**, *6*, 61.
10. Chalmpes, N.; Bourlinos, A.B.; Talande, S.; Bakandritsos, A.; Moschovas, D.; Avgeropoulos, A.; Karakassides, M.A.; Gournis, D. Nanocarbon from rocket fuel waste: the case of furfuryl alcohol-fuming nitric acid hypergolic pair. *Nanomaterials* **2021**, *11*, 1.
11. Chalmpes, N.; Moschovas, D.; Tantis, I.; Bourlinos, A.B.; Bakandritsos, A.; Fotiadou, R.; Patila, M.; Stamatis, H.; Avgeropoulos, A.; Karakassides, M.A.; et al. Carbon nanostructures derived through hypergolic reaction of conductive polymers with fuming nitric acid at ambient conditions. *Molecules* **2021**, *26*, 1595.
12. Chalmpes, N.; Moschovas, D.; Bourlinos, A.B.; Spyrou, K.; Vasilopoulos, K.C.; Avgeropoulos, A.; Karakassides, M.A.; Gournis, D. Hypergolic ignition of 1,3-cyclodienes by fuming nitric acid toward the fast and spontaneous formation of carbon nanosheets at ambient conditions. *Micro* **2021**, *1*, 15-27.
13. El-Sayed, A. Fundamentals of Aircraft and Rocket Propulsion (Chapter 11th). In: Fundamentals of Aircraft and Rocket Propulsion. Springer, London.; 2016.
14. Pratsinis, S.E. Flame aerosol synthesis of ceramic powders. *Progress in Energy and Combustion Science* **1998**, *24*, 197-219, doi:https://doi.org/10.1016/S0360-1285(97)00028-2.
15. Lan, Y.; Lu, Y.; Ren, Z. Mini review on photocatalysis of titanium dioxide nanoparticles and their solar applications. *Nano Energy* **2013**, *2*, 1031-1045.
16. Schneider, J.; Matsuoka, M.; Takeuchi, M.; Zhang, J.; Horiuchi, Y.; Anpo, M.; Bahnemann, D.W. Understanding TiO_2 photocatalysis: mechanisms and materials. *Chemical Reviews* **2014**, *114*, 9919-9986.
17. Hanaor, D.A.H.; Sorrell, C.C. Review of the anatase to rutile phase transformation. *Journal of Materials Science* **2011**, *46*, 855-874.

18. Ohno, T.; Sarukawa, K.; Tokieda, K.; Matsumura, M. Morphology of a TiO_2 Photocatalyst (Degussa, P-25) consisting of anatase and rutile crystalline phases. *Journal of Catalysis* **2001**, *203*, 82-86.
19. Su, R.; Bechstein, R.; Sø, L.; Vang, R.T.; Sillassen, M.; Esbjörnsson, B.; Palmqvist, A.; Besenbacher, F. How the anatase-to-rutile ratio influences the photoreactivity of TiO_2. *The Journal of Physical Chemistry C* **2011**, *115*, 24287-24292.
20. He, J.; Du, Y.-e.; Bai, Y.; An, J.; Cai, X.; Chen, Y.; Wang, P.; Yang, X.; Feng, Q. Facile formation of anatase/rutile TiO_2 nanocomposites with enhanced photocatalytic activity. *Molecules* **2019**, *24*, 2996.
21. Estrada Flores, M.; Reza, C.; Salmones, J.; Wang, J.A.; Manríquez, M.E.; Mora-Hernandez, J.; Hernández, M.; Zúñiga, A.; Contreras, J. Synthesis of nanoporous TiO_2 thin films for photocatalytic degradation of methylene blue. *Journal of New Materials for Electrochemical Systems* **2014**, *17*.
22. Xing, Z.; Zhou, W.; Du, F.; Zhang, L.; Li, Z.; Zhang, H.; Li, W. Facile synthesis of hierarchical porous TiO_2 ceramics with enhanced photocatalytic performance for micropolluted pesticide degradation. *ACS Applied Materials & Interfaces* **2014**, *6*, 16653-16660.
23. Tsirka, K.; Katsiki, A.; Chalmpes, N.; Gournis, D.; Paipetis, A.S. Mapping of graphene oxide and single layer graphene flakes—defects annealing and healing. *Frontiers in Materials* **2018**, *5*.
24. Pakade, V.E.; Tavengwa, N.T.; Madikizela, L.M. Recent advances in hexavalent chromium removal from aqueous solutions by adsorptive methods. *RSC Advances* **2019**, *9*, 26142-26164.
25. Shaban, Y. Effective photocatalytic reduction of Cr(VI) by carbon modified (CM)-n-TiO_2 nanoparticles under solar irradiation. *World Journal of Nano Science and Engineering* **2013**, *03*, 154-160.
26. Ali, M.E.M.; Assirey, E.A.; Abdel-Moniem, S.M.; Ibrahim, H.S. Low temperature-calcined TiO_2 for visible light assisted decontamination of 4-nitrophenol and hexavalent chromium from wastewater. *Scientific Reports* **2019**, *9*, 19354.
27. Asimakopoulos, G.; Baikousi, M.; Salmas, C.; Bourlinos, A.B.; Zboril, R.; Karakassides, M.A. Advanced Cr(VI) sorption properties of activated carbon produced via pyrolysis of the "Posidonia oceanica" seagrass. *Journal of Hazardous Materials* **2021**, *405*, 124274.
28. Asimakopoulos, G.; Baikousi, M.; Kostas, V.; Papantoniou, M.; Bourlinos, A.B.; Zbořil, R.; Karakassides, M.A.; Salmas, C.E. Nanoporous activated carbon derived via pyrolysis process of spent coffee: structural characterization. Investigation of its use for hexavalent chromium removal. *Applied Sciences* **2020**, *10*, 8812.
29. Chi, Y.; Tian, C.; Li, H.; Zhao, Y. Polymerized titanium salts for algae-laden surface water treatment and the algae-rich sludge recycle toward chromium and phenol degradation from aqueous solution. *ACS Sustainable Chemistry & Engineering* **2019**, *7*, 12964-12972.